High capacity gas capture and selectivity properties of triazatruxene-based ultramicroporous hyper-crosslinked covalent polymer

Ali Enis SADAK* ⓘ

Chemistry Group Laboratories, TUBITAK National Metrology Institute (NMI), Kocaeli, Turkey

Abstract: Tuning the selective sorption features of microporous organic networks is of great importance for subsequent applications in gas uptake and hiding, while it is more attractive in terms of being both time and cost effective to realize these optimizations without using functional groups in the core and linker. "Knitting" is one of the easiest and most used method to obtain a broad scope of hyper-crosslinked polymers on a large scale from aromatic structures that do not contain functional groups for polymerization. By the use of Knitting method, a hypercrosslinked covalent ultramicroporous organic polymer was obtained via stepwise process from using triazatruxene (TAT) as core -a planar indole trimer- through anhydrous $FeCl_3$ catalyzed Friedel–Crafts alkylation using dimethoxybenzene as a linker. The resulting microporous polymer, namely TATHCCP was completely identified by analytical and spectral techniques after examined for gas properties (CO_2, CH_4, O_2, CO, and H_2) and selectivity (CO_2/N_2, CO_2/O_2, for CO_2/CO and CO_2/CH_4) up to 1 bar and increased temperatures (273 K, 296 K and 320 K). Although it has a relatively low (Brunauer–Emmett–Teller) BET specific surface area around 557 m^2/g, it was seen to have a high CO_2 capture capacity approaching 10% wt. at 273 K. In accordance with (ideal adsorbed solution theory) IAST computations, it was revealed that interesting selectivity features hitting up to 60 for CO_2/N_2, 45 for CO_2/O_2, 35 for CO_2/CO, 13 for CO_2/CH_4 at lower temperatures revealed that the material has much better selectivity values than many HCP (hyper-crosslinked polymer) derivatives in the literature even from its most similar analog dimethoxymethane derivative TATHCP, which has a surface area of 950 m^2/g.

Key words: Friedel-Crafts, IAST (ideal adsorbed solution theory), microporous organic polymer, triazatruxene, hyper-crosslinked polymers, gas uptake

1. Introduction

Except for a small portion of the energy currently used worldwide, such as 13%, the remainder is obtained by using fossil fuels. As a result of this high energy need, which causes climate change with high CO_2 emissions, a wide variety of CO_2 capture and separation techniques are being developed. In addition to the chemical CO_2 capture process of the currently used amine solutions (diluted with 70% water) that are toxic, corrosive and degradation over time, the highly porous recyclable polymers that work according to the physisorption process are highly promising [1]. By increasing the surface area and addition of electron rich atoms on these materials, CO_2 uptake and selectivity are increased, as well as the capture affinity for other pipe gases (a pipe gas includes SO_x (<800 ppm), NO_x (<500 ppm), O_2 (3%–4%), H_2O (5%–7%), CO_2 (15%–16%) and N_2 (75%–76%)) can be practically changed [2]. Increased hydrogen bonding ability and dipole quadrupole interactions by using polar groups such as amine, hydroxyl and halogen of the porous material surface can capture CO_2 gas more selectively on N_2 and CH_4 [3]. Accordingly, synthesis of new porous materials using nitrogen-rich monomers and combination of polar groups into their construction through post modification techniques are of great interest [4,5]. Microporous organic polymers consisting of light nonmetallic elements with large surface area, narrow pore size, and high degree of thermal and chemical stability are extremely low-cost cutting-edge materials used for gas sorption and storage processes. Examples of many microporous polymers with high gas capture and separation capacities include triazine derivative crystalline organic networks (CTFs) [6,7], covalent organic networks (COFs) [8], microporous conjugated polymers (CMPs) [9,10], intrinsic microporosity polymers (PIMs) [11,12], porous aromatic frameworks (PAFs) [13] and hypercrosslinked polymers (HCPs) [14–17] can be given. Hyper-covalent conjugated polymers (HCCPs), another subclass of MOPs, differ from HCPs due to their conjugation. Although the synthesis methods are similar to HCPs, it has

* Correspondence: alienis.sadak@tubitak.gov.tr

been found that HCCPs are more effective especially in gas selectivity thanks to their continuous conjugation due to the use of aromatic linkers in their synthesis [14]. Triazatruxene, which contains three nitrogen atoms that highly effective in gas capture processes, is an important indole derivative due to its planar and aromatic structure, as well as active benzene rings in Friedel–Crafts alkylation reaction. Triazatruxene derivatives have a great interest as a result of their high electron supply capability provided by the p-conjugate structure with high electron mobility and thermal stability provided in complex structures [18–22]. It was observed by our group that the HCP derivative of triazatruxene (TATHCP) synthesized by using the methylal linker has a high degree of gas adsorption and selectivity [15]. Therefore, in this study in order to see how change the gas uptake and selectivity properties of TATHCP by the change of linker, the synthesis, gas uptake and selectivity properties of the hypercovalent conjugated structure TATHCCP was obtained by using dimethoxybenzene as linker and triazatruxene as core. Despite the lower surface area of TATHCCP compared to its analog TATHCP, there is notable increase of CO_2 selectivity over N_2, CH_4 and CO of TATHCCP, which shows the obvious difference on the use of aromatic linker in the selectivity.

2. Materials and methods

2.1. Materials
$POCl_3$ 99% purity was purchased from Sigma-Aldrich (Sigma-Aldrich Corp., St. Louis, MO, USA). 2-oxoindole 97% purity was procured from Sigma-Aldrich. Dimethoxymethane reagent plus 99% purity was purchased from Sigma-Aldrich. KOH ≥ %85 purity was purchased from Merck. All materials were used as received, unless otherwise stated.

2.2. 10,15-Dihydro-5H-diindolo[3,2-a:3',2'-c]carbazole (Triazatruxene, 2)
In a 50 mL round-bottomed flask there was added 2-oxoindole (1; 2 g, 15 mmol) into $POCl_3$ (10 mL, 105 mmol) stirred until dissolved at RT then stirred at 100 °C for 8 h. After 8 h, reaction mixture was cooled to room temperature and poured into a 500 mL beaker containing ice chips (250 mL) and saturated KOH was added until the pH value reached 7. The resulting dark green colored settlings were collected by vacuum filtration using No. 2 sintered glass filtrate and the raw product (1.2 g) was purified by silica gel (150 g) column chromatography by using 4:1 ethyl acetate/hexane as the eluent. After crystallization from 4:1 acetone/hexane, 10,15-dihydro-5H-diindolo[3,2-a:3',2'-c]carbazole (2) was obtained (Yield: 40%, 0.8 g) [23]. Melting point: 393-394 °C. ^{1}H-NMR (600 MHz, DMSO): d 11.86 (bs, 3H), 8.67 (d, J = 7.6 Hz, 3H), 7.73 (d, J = 7.6 Hz, 3H), 7.40 – 7.32 (m, 6H). APT ^{13}C-NMR (150 MHz, DMSO): d 139.0, 134.2, 123.0, 122.7, 120.3, 119.5, 111.4, 101.0. IR (KBr, cm^{-1}): 3473, 3439, 3053, 3025, 2919, 2852, 1737, 1635, 1273, 729.

2.3. 5,10,15-triethyl-10,15-dihydro-5H-diindolo[3,2-a:3',2'-c]carbazole (3)
In a 100 mL anhydrous THF, triazatruxene (2; 1.85 g, 5.36 mmol) and KOH (4.51 g, 80.34 mmol, 15 eq.) was added at room temperature and mixture was heated at 70 °C for 3.5 h. After cooling room temperature, ethyl bromide (2.33 g, 21.42 mmol, 4eq.) was added to the mixture. The mixture was stirred magnetically overnight at room temperature. After checking with TLC and understanding that the reaction was complete, solvent was removed under reduced pressure. The raw product was dissolved in 150 mL of EtOAc and washed with diluted $NaHCO_3$ (1× 100 mL) then water (3 × 100 mL) and dried over $MgSO_4$. The solvent was removed under reduced pressure. The raw product was purified on silica gel (20 g) column chromatography by using 1:4 CH_2Cl_2/hexane. After crystallization over acetone, 5,10,15-triethyl-10,15-dihydro-5H-diindolo[3,2-a:3',2'-c]carbazole (3) was obtained. (Yield: 89%, 2.1 g) ^{1}H-NMR (600 MHz, CDCl$_3$): δ ppm 8.37 (d, J = 8.0 Hz, 3H), 7.68 (d, J = 8.0 Hz, 3H), 7.48 (t, J = 7.4 Hz, 3H), 7.37 (t, J = 7.4 Hz, 3H), 5.05 (t, J = 7.2 Hz, 6H), 1.64 (t, J = 7.2 Hz, 9H). ^{13}C-NMR (150 MHz, CDCl$_3$): δ ppm 143.4, 141.4, 126.2, 125.4, 124.1, 122.5, 113.0 105.9, 44.4, 18.2. IR (powder, cm^{-1}): 3045, 2970, 1555, 1480, 1320, 1233, 1098, 724. HRMS: m/z: Calcd. for ($C_{30}H_{27}N_3$) [M+H$^+$]: 430.22385; found, 430.22868.

2.4. Synthesis of TATHCCP
In 20 mL nitrobenzene, 5,10,15-triethyl-10,15-dihydro-5H-diindolo[3,2-a:3',2'-c]carbazole (3) (0.250 g, 0.582 mmol) and p-dimethoxybenzene (1.210 g, 8.73 mmol, 15 equiv.) in 20 mL 1,2-dichloroethane, anhydrous $FeCl_3$ (4.150 g, 25.61 mmol, 44 equiv.) was added at room temperature. The mixture was stirred at 80°C for 5 h then at 120°C for 24 h under an inert (N_2) atmosphere. After 24 h, reaction mixture was cooling to room temperature then the dark brown precipitate was collected by using No. 1 sintered glass filtrate and repeatedly washed with methanol, concentrated HCl, distilled water, and methanol to eliminate unreacted monomers and $FeCl_3$ till the filtrate was almost colorless. Then, the TATHCCP was purified by Soxhlet extraction from THF (50 mL) for 24 h then dried under vacuum at 120 °C for 24 h to give dark brown-colored solid powder (Yield: 551 mg, 97 %). IR (powder, cm^{-1}): 2927, 1572, 1457, 1427, 1324, 1208, 1135, 852, 811.

3. Results and discussion

3.1. Synthesis and characterization

One of the easiest methods to obtain a broad diversity of hyper-crosslinked polymers on a large scale by using aromatic structures that do not including active groups for polymerization is known as the "knitting" method [24,25]. Here, a new hyper-crosslinked covalent polymers network called TATHCCP is introduced, which obtained with Friedel-Crafts alkylation using triazatruxene (TAT) as the core and dimethoxymethane as the external linker (Figure 1a). Like the other similar HCPs synthesized using the same knitting method, the yield of TATHCCP was also quantitative [24,26]. The triazatruxene ring was obtained in a similar way to the previous work [23], and N-alkylation of the nitrogen atoms of the trimer structure was performed with ethyl bromide to increase the solubility (Figure 1a). By increasing the equivalent amounts of catalyst from 3 equivalents to 40 equivalents, the surface area of the obtained TATHCCP increased from 40 m^2/g to 557 m^2/g. The stability of the obtained TATHCCP polymer in water and most organic solvents even in diluted NaOH and HCl simplified the purification and activation steps.

3.2. Textural and spectral properties

FT-IR, SEM, TEM, XRD, and solid-state magic angle spinning (CP/MAS) ^{13}C NMR spectrometry were used to examine of the spectral properties of obtained material, as shown in Figure 2 and Figure S1-S10, SI. FT-IR peaks show the C−N−C moieties appear as characteristic bands at around 1450 cm^{-1} while aromatic C=C bands (stretching) vibrations around 850–1580 cm^{-1} which belong to carbazole pyrrole fused benzene rings and crosslinked benzene moieties. C−H vibrations (stretching) around 2927 cm^{-1} indicate that the material is appropriate with the supposed cross-linked polymer (Figure 2). ^{13}C CP-MAS NMR spectroscopy was utilized to further support the chemical structure of the TATHCCP (Figure S1, SI). Peaks resonance at 143 and 127 ppm belong to fused carbazole rings of TAT, while the peak near 57 ppm belongs to
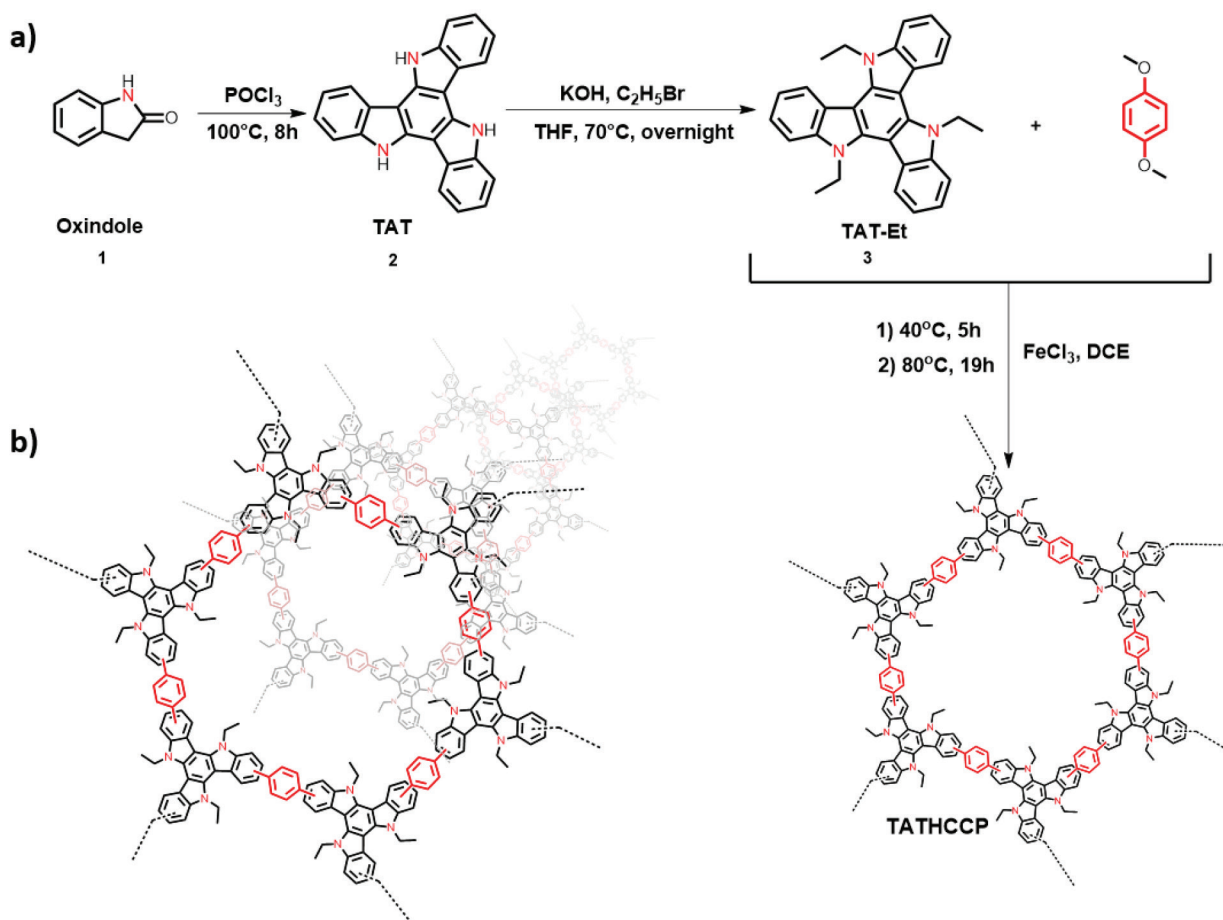

Figure 1. a) Synthesis of TAT-HCCP. b) Proposed structure of TAT-HCCP (the actual structure can be much more complex due to the dense crosslinking).
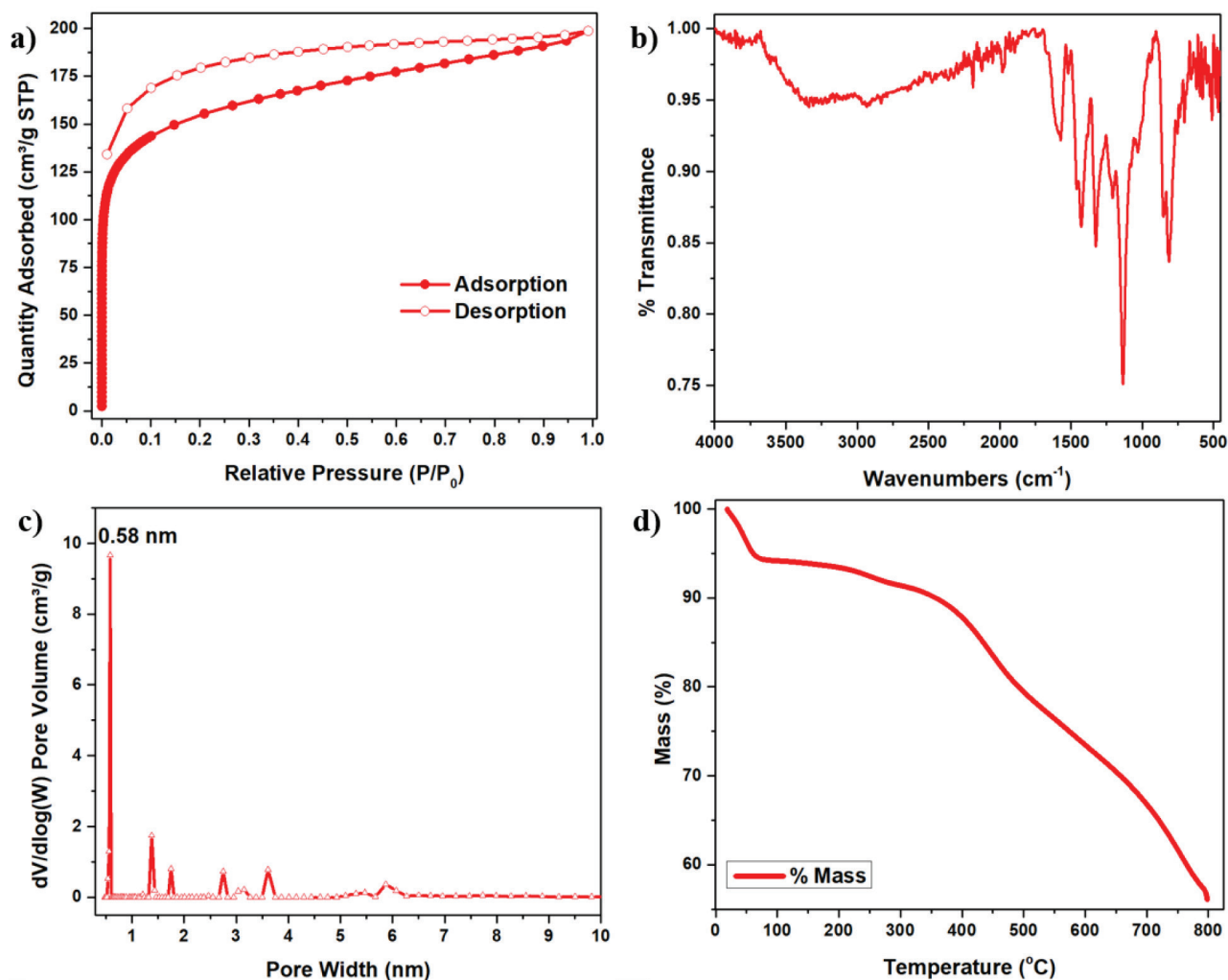
Figure 2. Structural characterization of TATHCCP (a) N2 adsorption-desorption isotherms at 77 K, (b) FT-IR spectrum, (c) pore size distribution, (d) thermogravimetric analysis.

carbon in unreacted methoxy group of dimethoxybenzene crosslinker showing the uncompleted reaction of TATHCCP. In addition, unsubstituted aromatic carbons of dimethoxybenzene have resonance at 157 ppm while the peak of the carbon atoms at the 3-position of the indole trimer a resonance at about 106 ppm (Figure S1, SI). Asterisks denote at 217, 188, 117, and 95 ppm are denoted spinning sidebands. SEM and EDX analysis was examined for particle composition and purity of the TATHCCP polymer. From SEM images of polymer, the findings suggest formation of submicrometer size of aggregated particles, while EDX analysis showed that there was not $FeCl_3$ catalyst in the polymer obtained, except for C and N elements and O element from unreacted dimetoxymethane moiety. (Figure 3, SI). The powder XRD spectrum has not indicate any typical peaks showing that the polymer has greatly amorphous character (Figure S2, SI).

It is seen from the thermogravimetric analysis (TGA) spectrum that the polymer has a thermal stability up to 350 °C, and it is also seen that it retains 50% of its mass up to 800 °C (Figure 2d). Possible reason of this significant retain from the mass of TATHCCP is N-doped carbon because of thermal disintegration. Because of residuary solvent and moisture evaporation there is an initial weigh loss near at 90 °C. Considering the results of the TGA analysis, it is seen that TATHCCP is a possible candidate as it meets the requirements in high temperature processes such as CO_2 capture and post combustion.

3.3. Porosity

Surface area and porosity of TATHCCP network were characterized at 77 K by using N_2 as probe gas. Activation of the polymer was achieved by degassing for 12 h at 200 °C to start the analysis. As can be seen from the N_2 adsorption desorption isotherm in Figure 2a, the sharp uptake at the initial low relative pressure (0−0.1 = P/P$_o$) region and above 0.1

at higher relative pressure shows that TATHCCP has a highly microporous character as well as a permanent microporosity. Considering the IUPAC [27] classification, it is seen that TATHCCP exhibits mixture of type I and V isotherm identity at increased pressures (Figure 2a). TATHCCP shows a mild capillary condensation between P/P$_o$ 0.9−0.95 that is commonly presented in microporous networks owing to distension force of the structure throughout the touch of interstitial gaps by the adsorbate molecules in the network [28]. The lack of edged adsorption peak at 0.8−1.0 P/P$_o$ high relative pressure area that points out the macroporous character reveals that TATHCCP doesn't have this kind of pore structures (Figure 2a). Calculated surface area analysis from the Langmuir (S$_{Lang}$) and BET (S$_{BET}$) (Brunauer – Emmett – Teller) theories and textural properties are given in Table 1. According to Langmuir model, surface area of the TATHCCP was found 702 m^{2}g^{-1}, while it was found 557 m^{2}g^{-1} for Brunauer – Emmett – Teller model as shown in Figures S3, SI and Figures S4, SI. The findings taken from pore size distribution graph (PSD) by using the nonlocal density functional theory (NLDFT) showed that the network has immensely (> 60%) ultramicropore character at 0.6 nm that promising for gas uptake and selectivity processes (Figure 2c).

Total pore and micropore volume of TATHCCP was found 0.31 and 0.26, respectively at relative pressures P/P0 = 0.99 and 0.1. By using the ratio of micropore volume to total pore volume, degree of microporosity of TATHCCP was calculated as 84%, which is quite high compare with it's before synthesized hyper covalent analog TATHCP (%70).

3.4. Gas uptake and selectivity

The amazing degree of microporosity (83%) with high amount of electron rich nitrogen bones of TATHCCP was encouraging to examine comprehensively for the possibility of promising gas uptake properties. Five different gas including
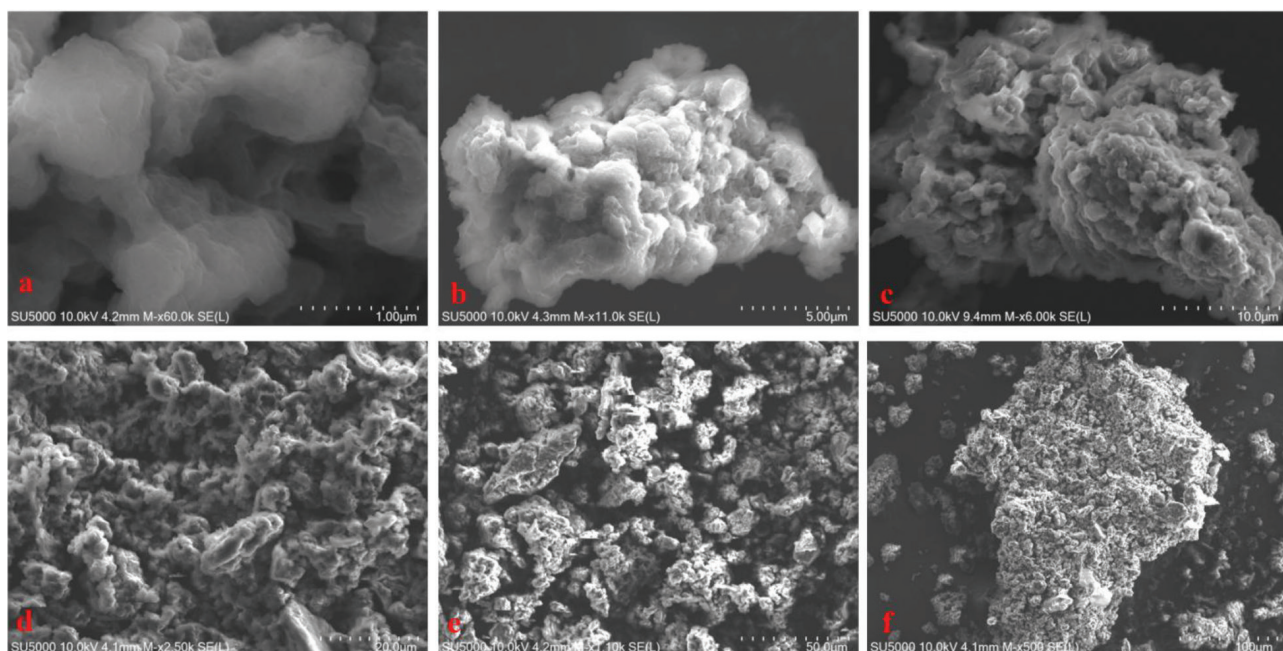

Figure 3. SEM images of TATHCCP (a–f). See SI for more images.

Table 1. The textural properties of the TATHCCP.

Polymer	S$_{BET}$[a] [m^{2}g^{-1}]	S$_{Lang}$[b] [m^{2}g^{-1}]	S$_{micro}$[c] [m^{2}g^{-1}]	V$_t$[d] [cm^{3}g^{-1}]	V$_{0.1}$[e] (cm^{3}g^{-1})	%V$_{0.1}$/V$_t$	%S$_{micro}$/S$_{BET}$	4V/A$_{BET}$[f] [nm]
TATHCCP	557	702	345	0.31	0.26	84	62	2.20

a. BET surface area calculated from N$_2$ adsorption isotherm in the relative pressure (P/P$_0$) range from 0.05 to 0.20. b. Langmuir surface area calculated from N$_2$ adsorption isotherm in the pressure range from 30 to 220 mbar. c. Micropore surface area calculated from the N$_2$ adsorption isotherm using t-plot method from the Harkins–Jura equation. d. Total pore volume at P/P$_0$ = 0.99. e. Micropore volume at P/P$_0$ = 0.1. f. Average pore diameter.
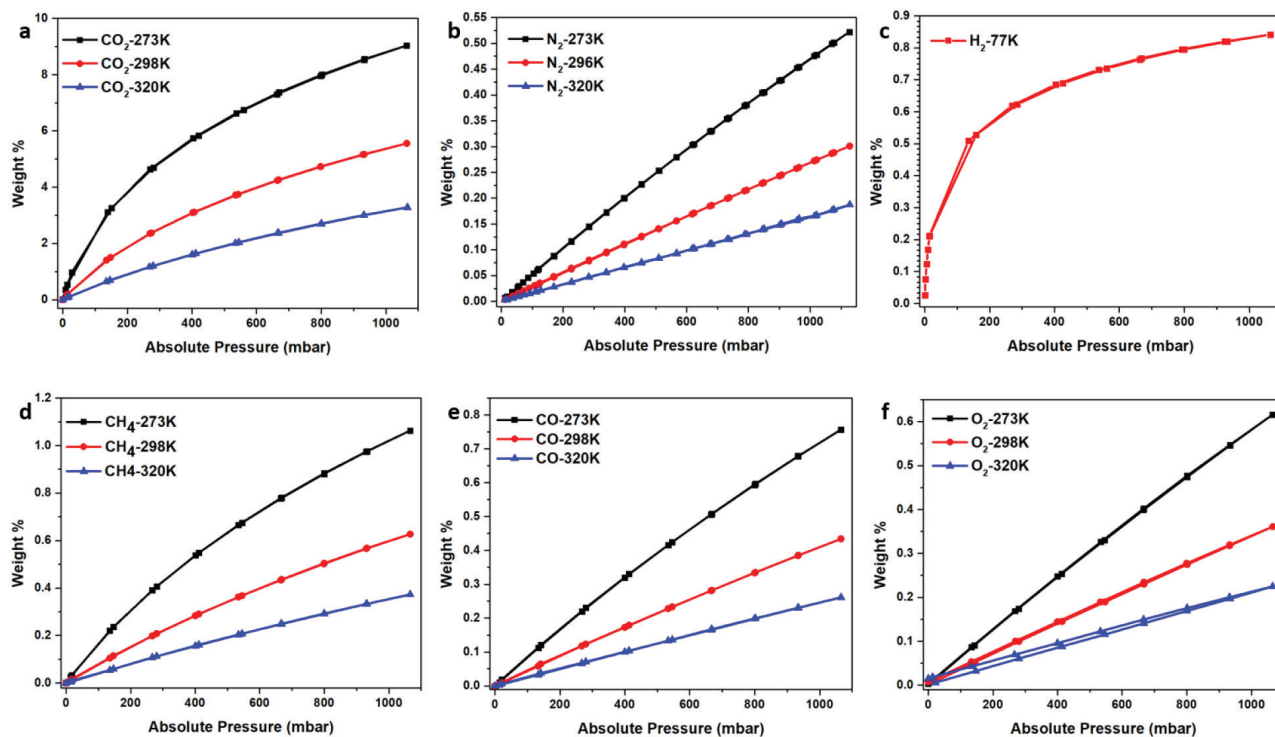
Figure 4. Gas uptake (weight %) properties of TATHCCP. (a) CO_2, (b) N_2, (c) H_2, (d) CH_4, (e) CO, (f)O_2 CO adsorption-desorption isotherms at 273K, 298K and 323 K.

CO_2, N_2, CH_4, CO, and O_2 was used to determine the adsorption properties of TATHCCP from 0 to 1.1 bar pressures at 273 K, 298 K, and 320 K (Figure 4, Table S1). CO_2 uptake capacity of TATHCCP was found 9.0% by weight at 273K /1.1 bar, 5.5% by weight at 298 K /1.1 bar, and 3.2% by weight at 298K /1.1 bar, respectively (Figure 4a) . CO_2 physisorption process seems reversible as the desorption isotherms are very close to adsorption isotherms. Although TATHCCP has a moderate surface area with respect to its hyper covalent analog TATHCP, obtained CO_2 uptake values are very close to TATHCP at all temperature, and higher or closer than lots of networks with nearly equal surface area in literature (Table S3) [1, 29–34]. Main effect of this high CO_2 adsorption capacity of TATHCCP is due to the lone pair electrons of high amount nitrogen atoms on network, which are used to catch CO_2 molecules with hydrogen bonding. In contrast to CO_2 adsorption values, N_2 adsorption values of TATHCCP were found very low at all three temperatures, which can be summarized as the TATHCCP has highly N_2 phobic character. N_2 uptake capacity of TATHCCP was found 0.52 wt%, 0.30 wt% and 0.18 wt% at 273 K, 298 K and 320 K at 1.1 bar, respectively (Figure 4b).

The Clausius–Clapeyron equation was used to obtain the isosteric heat of adsorption (Q_{st}) values of TATHCCP to determine whether CO_2 is physically adsorbed. Calculated Q_{st} values of TATHCCP was found 34.7 kJ mol^{-1} at zero loading and the fact that it remained as 29.5 kJ mol^{-1} even when the adsorbed amount of CO_2 increased reveals that the network has well retention ability despite the low surface area (Figure S8, SI). Additionally, TATHCCP physically adsorbs CO_2 molecules due to the Q_{st} values not more than 50 kJ mol^{-1}, and thanks to the weak interactions with CO_2, the network has a good recycle ability, which needs no more energy. Compared to low pressure and compressed form, physically adsorbed CH_4 storage utilities are safer for long transportation processes and in terms of cost. Moreover, in clean energy applications, the physically adsorption of hydrogen is of great interest. Even if much higher pressures are needed to determine the exact gas uptake values for H_2 and CH_4 adsorption, low pressure uptakes up to 1 bar help to see latter gas separation utilities. Therefore, the adsorption properties of TATHCCP were tested by using H_2 at 77 K and CH_4 at 283, 298, and 320 K as probe gases. H_2 adsorption value of TATHCCP was found 0.84 wt % at 77 K, while CH_4 adsorption values was found 1.06 wt%, 0.62 wt% and 0.37 wt% at 283, 298, and 320 K at 1.1 bar separately (Figures 4c, 4d). It is understood that higher H_2 capacity can be obtained at higher pressures as saturation cannot be reached as seen from the H_2 isotherm of TATHHCCP performed at 77K. Also, this H_2 uptake values are remarkable when compared with previous works [35–38] (Table S4). The obtained CH_4 uptake values of TATHCCP are comparable with the previous works [28, 36, 39–45] (Table S5). Also, the calculated Q_{st} values of CH_4 by using isotherm data at 273 and 298 K (Figure S9) indicate that TATHCCP has 23.31 kJ

mol^{-1} at zero coverage. Difference between the Q_{st} values of CH_4 and CO_2 is due to the nonpolar character of CH_4, which has a less interaction with polymer compared with CO_2 molecules.

TATHCCP adsorption capacity was also examined by using CO and O_2 as probe gases separately at 273 K, 298 K, and 320 K at 1.1 bar before calculation of selectivity properties. CO adsorption values of TATHCCP was found 0.75 wt%, 0.43 wt%, 0.26 wt% at 273, 298, and 320 K while O_2 uptake values was found 0.61 wt%, 0.36 wt%, and 0.22 wt% at 273, 298, and 320 K at 1.1 bar, respectively (Figures 4e, 4f).

Besides, high CO_2 sorption values, recycle ability, and CO_2 selectivity over other pipe gases have the most important subjects of a new porous material candidate for using post combustion processes. Myers and Prausnitz's ideal adsorbed solution theory (IAST) is one of the most used technique for prediction of adsorption feature from using one-ingredient gas isotherms to calculate multi-components [46]. IAST was used to compute the CO_2 selectivity properties of TATHCCP over four different gases (CH_4, N_2, CO, and O_2) at the three different temperatures (273, 298, and 320 K) used for adsorption analysis up to 1 bar (Figures 5, 6 and Table S2). To see the minor differences, CO_2/N_2 selectivity of TATHCCP was calculated at three different pipeline ratios (05/95, 15/85, and 50/50) (Figures 5a, 5b). Additionally, CO_2/CH_4 selectivity of TATHCCP was calculated at two different ratios (05/95 and 50/50) while CO_2/CO and CO_2/O_2 selectivities were calculated at 50/50 ratio (Figure 6a, b). CO_2/N_2 selectivity values of TATHCCP were found 59.1, 28.5, and 18.3 at 50/50 ratio, while they were found 50.0, 25.9, 18.3 at 15/85 ratio and 49.2, 25.9, 18.2 at 05/95 ratio at 273 K, 298 K and 320 K at 1.1 bar pressure, respectively (Figure 5a). Obtained selectivity values of TATHCCP at three different ratios and temperatures are close to each other and higher than previous networks in literature and especially its hypercovalent analog TATHCP [47–51] (Table S2, S6, SI).

Selectively separation of CO_2 from CH_4 is very important issue in the purification process of natural gas due to preventing of pipeline corrosion and rise of obtained energy yield [28]. CO_2/CH_4 selectivities of TATHCCP at 50/50 ratio were found 12.3, 5.4, and 4.4, while they were found as 9.7, 5.9, and 4.5 at 05/95 ratio at 273 K, 298 K, 320 K at 1.1 bar pressure, respectively (Figure 5b). Obtained CO_2/CH_4 selectivities at 05/96 ratio of TATHCCP are nearly the same of its analog TATHCP at all three degrees and higher than most of the previous works at 273 K (Table S7) [47,52,53].

CO_2/CO and CO/O_2 selectivities of TATHCCP were also calculated at the same temperatures and pressure as to compare to TATHCP and previous works. Calculated CO_2/CO selectivities of TATHCCP were found as 35.0, 17.6, and 12.3 at 50/50 ratio at temperatures 273, 296, and 320 K at 1.1 bar, respectively while CO_2/O_2 selectivies were found 45.9, 23.5, and 16.4 at the same temperatures and pressure (Figures 6a, 6b). Both of CO_2 selectivities over CO and O_2 of TATHCCP at 273 K are higher than its analog TATHCP while a little low at other two temperature (Table S2). When TATHCCP (557 m^2/g) and TATHCP (997 m^2/g) obtained from the same triazatruxene core are compared considering the selectivity results, its obviously seen that specific surface area is not the main effect of selectivity. Continuous resonance of TATHCCP is one of the possible reasons of high selectivity values than TATHCP, and the other one is probably due to higher degree of microporosity of TATHCCP (%84) compared to TATHCP (%70), which helps to more selective CO_2
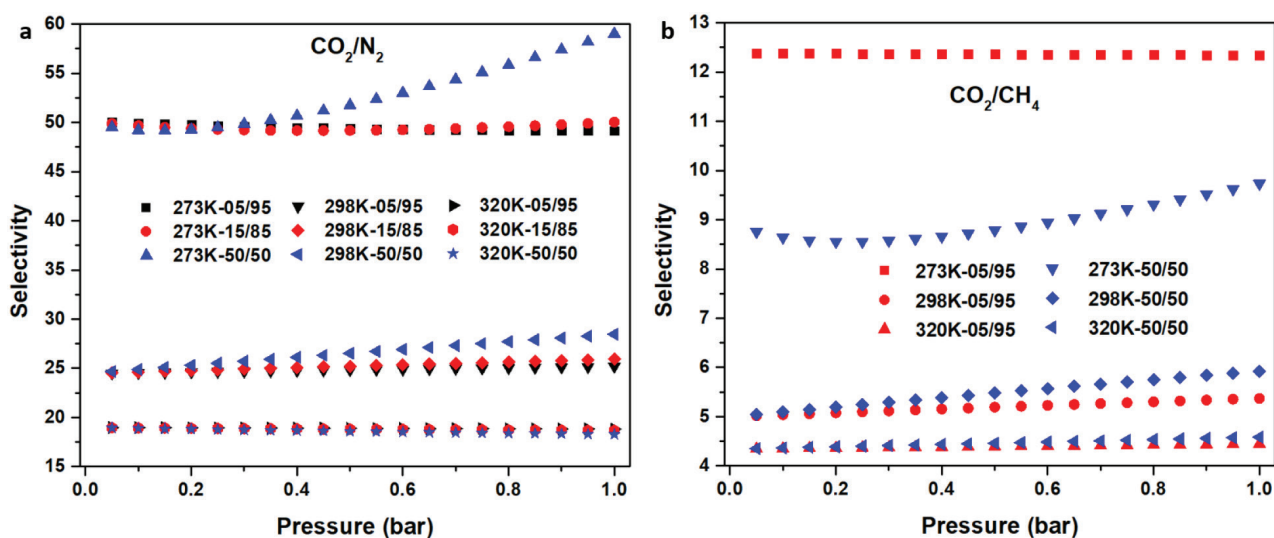

Figure 5. Selectivity calculations of TATHCCP using the IAST for (a) CO_2/N_2-05/95, 15/85, and 50/50 at 273 K, 296 K, and 320 K, (b) CO_2/CH_4-05/95 and 50/50 at 273 K, 296 K, and 320 K.
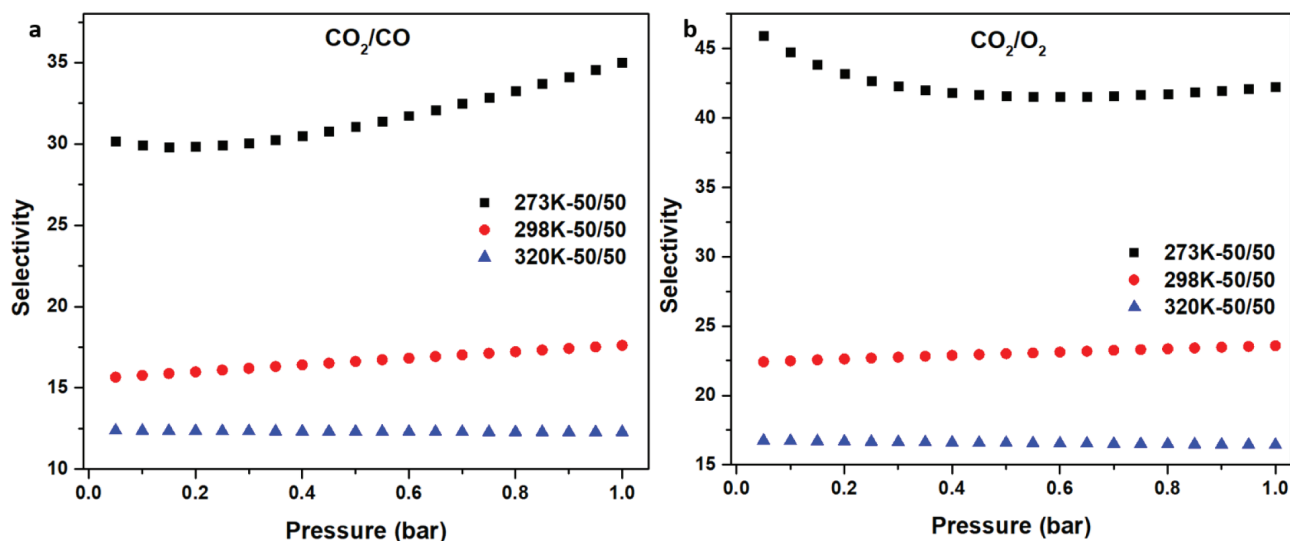
Figure 6. Selectivity calculations of TATHCCP using the IAST for (a). CO_2/CO-50/50 at 273 K, 296 K and 320 K. (b). CO_2/O_2-05/95 and 50/50 at 273 K, 296 K, and 320 K.

catching. These differences in selectivity and sorption properties observed between these two hypercovalent polymers based on triazatruxene cannot be generalized for all hypercovalent polymers that consist of the same core but contain only differentiated linkers. Each polymer obtained with high porosity has its own selectivity and sorption properties arising from the core from which it is formed. It's known from previous studies of HCP derivatives that even if the change of linkers affects the selectivity properties, the core of the polymer and the different atoms attached to the core also affect the selectivity values of the obtained polymers [14,54]. Therefore, regardless of whether the linkers used in different studies are the same, if the core used is different from the one used in the other study, the selectivity and sorption properties should be examined from the beginning. In this way, changes can be observed much more clearly by both the linker and the core. This study has been one of the rare studies in which these differences are shown specifically for linkers.

4. Conclusion

In sum, starting from electron-rich triazatruxene and using aromatic dimethoxybenzene ring as a linker, a new microporous hypercrosslinked conjugated polymer, TATHCCP, was synthesized by using $FeCl_3$ catalyzed Friedel–Crafts reaction. The high degree of micropore character of 84%, together with the moderate surface area, prompted the study of TATHCCP's gas uptake and selectivity properties. The gas uptake properties are comparable to most of the similar structures in the literature, as well as higher selectivity properties than many of the previously synthesized HCPs and especially its previous analog TATHCP, revealed that TATHCCP has a high potential for CO_2 separation processes in flue gas systems. The obtained Q_{st} values in the physical adsorption region for CO_2 and CH_4, its resistance to highly acidic-basic environments and different solvents combined with its cheap structure make TATHCCP very useful for industrial applications. Furthermore, this study showed how the degree of microporosity also plays an important role, as well as the effect of high specific surface area on selectivity properties.

Supplementary materials

Materials and methods, synthesis, Langmuir and BET area plots, scanning electron microscopy (SEM) images, energy-dispersive X-ray spectroscopy (EDS) images and spectra, solid-state ^{13}C CP-MAS NMR spectra, adsorption selectivities of CO_2 over N_2, CH_4, O_2, CO, tables of selectivity, gas adsorption capacity and CO_2, CH_4, H_2 uptake comparison of different microporous materials.

References

1. Liebl MR, Senker J. Microporous functionalized triazine-based polyimides with high CO_2 capture capacity. Chemistry of Materials 2013; 25: 970-980.

2. Dawson R, Cooper AI, Adams DJ. Chemical functionalization strategies for carbon dioxide capture in microporous organic polymers. Polymer International 2013; 62: 345-352.

3. Rabbani MG, El-Kaderi HM. Template-free synthesis of a highly porous benzimidazole-linked polymer for CO_2 capture and H_2 storage. Chemistry of Materials 2011; 23: 1650-1653.

4. Demessence A, D'Alessandro DM, Foo ML, Long JR. Strong CO_2 binding in a water-stable, triazolate-bridged metal– organic framework functionalized with ethylenediamine. Journal of the American Chemical Society 2009; 131: 8784-8786.

5. Lu W, Yuan D, Sculley J, Zhao D, Krishna Ret al. Sulfonate-grafted porous polymer networks for preferential CO_2 adsorption at low pressure. Journal of the American Chemical Society 2011; 133: 18126-18129.

6. Kuhn P, Forget A, Su D, Thomas A, Antonietti M. From microporous regular frameworks to mesoporous materials with ultrahigh surface area: dynamic reorganization of porous polymer networks. Journal of the American Chemical Society 2008; 130: 13333-13337.

7. Kuhn P, Antonietti M, Thomas A. Porous covalent triazine-based frameworks prepared by ionothermal synthesis. Angewandte Chemie International Edition 2008; 47: 3450-3453.

8. Xiang Z, Cao D. Porous covalent–organic materials: synthesis, clean energy application and design. Journal of Materials Chemistry A 2013; 1: 2691-2718.

9. Cooper AI. Conjugated microporous polymers. Advanced Materials 2009; 21: 1291-1295.

10. Jiang JX, Su F, Trewin A, Wood CD, Campbell NLet al. Conjugated microporous poly (aryleneethynylene) networks. Angewandte Chemie International Edition 2007; 46: 8574-8578.

11. Budd PM, Butler A, Selbie J, Mahmood K, McKeown NB et al. The potential of organic polymer-based hydrogen storage materials. Physical Chemistry Chemical Physics 2007; 9: 1802-1808.

12. McKeown NB, Budd PM. Polymers of intrinsic microporosity (PIMs): organic materials for membrane separations, heterogeneous catalysis and hydrogen storage. Chemical Society Reviews 2006; 35: 675-683.

13. Ben T, Ren H, Ma S, Cao D, Lan Jet al. Targeted synthesis of a porous aromatic framework with high stability and exceptionally high surface area. Angewandte Chemie 2009; 121: 9621-9624.

14. Sadak AE. A comparative gas sorption study of dicarbazole-derived microporous hyper-crosslinked polymers. Microporous and Mesoporous Materials 311: 110727.

15. Sadak AE, Karakuş E, Chumakov YM, Dogan NA, Yavuz CT. Triazatruxene-based ordered porous polymer: high capacity CO_2, CH_4, and H_2 capture, heterogeneous Suzuki–Miyaura catalytic coupling, and thermoelectric properties. ACS Applied Energy Materials 2020; 3: 4983-4994.

16. Wood CD, Tan B, Trewin A, Su F, Rosseinsky MJ et al. Microporous organic polymers for methane storage. Advanced Materials 2008; 20: 1916-1921.

17. Luo Y, Li B, Wang W, Wu K, Tan B. Hypercrosslinked aromatic heterocyclic microporous polymers: a new class of highly selective CO_2 capturing materials. Advanced Materials 2012; 24: 5703-5707.

18. Ji L, Fang Q, Yuan M-s, Liu Z-q, Shen Y-xet al. Switching high two-photon efficiency: from 3, 8, 13-substituted triindole derivatives to their 2, 7, 12-isomers. Organic Letters 2010; 12: 5192-5195.

19. Bura T, Leclerc N, Bechara R, Lévêque P, Heiser T et al. Triazatruxene-diketopyrrolopyrrole dumbbell-shaped molecules as photoactive electron donor for high-efficiency solution processed organic solar cells. Advanced Energy Materials 2013; 3: 1118-1124.

20. Ruiz C, Lopez Navarrete JT, Ruiz Delgado MC, Gómez-Lor B. Triindole-bridge-triindole dimers as models for two dimensional microporous polymers. Organic Letters 2015; 17: 2258-2261.

21. Shao J, Guan Z, Yan Y, Jiao C, Xu Q-Het al. Synthesis and characterizations of star-shaped octupolar triazatruxenes-based two-photon absorption chromophores. The Journal of organic chemistry 2011; 76: 780-790.

22. Lai WY, He QY, Zhu R, Chen QQ, Huang W. Kinked star-shaped fluorene/triazatruxene co-oligomer hybrids with enhanced functional properties for high-performance, solution-processed, blue organic light-emitting diodes. Advanced Functional Materials 2008; 18: 265-276.

23. Sadak AE, Gören AC, Bozdemir ÖA, Saraçoğlu N. Synthesis of novel meso-indole- and meso-triazatruxene-bodipy dyes. Chemistry Select 2017; 2: 10512-10516.

24. Xu S, Luo Y, Tan B. Recent development of hypercrosslinked microporous organic polymers. Macromolecular Rapid Communications 2013; 34: 471-484.

25. Shen R, Yan X, Guan Y-J, Zhu W, Li T et al. One-pot synthesis of a highly porous anionic hypercrosslinked polymer for ultrafast adsorption of organic pollutants. Polymer Chemistry 2018; 9: 4724-4732.

26. Sing KSW, Everett DH, Haul RAW, Moscou L, Pierotti RA et al. Reporting physisorption data for gas/solid systems with special reference to the determination of surface area and porosity (recommendations 1984). Pure and Applied Chemistry 1985; 57: 603-619.

27. Saleh M, Lee HM, Kemp KC, Kim KS. Highly stable CO_2/N_2 and CO_2/CH_4 selectivity in hyper-cross-linked heterocyclic porous polymers. ACS applied materials & interfaces 2014; 6: 7325-7333.

28. Ben T, Pei C, Zhang D, Xu J, Deng F et al. Gas storage in porous aromatic frameworks (PAFs). Energy & Environmental Science 2011; 4: 3991-3999.

29. Jeon HJ, Choi JH, Lee Y, Choi KM, Park JH et al. Highly selective CO_2-capturing polymeric organic network structures. Advanced Energy Materials 2012; 2: 225-228.

30. Jackson KT, Rabbani MG, Reich TE, El-Kaderi HM. Synthesis of highly porous borazine-linked polymers and their application to H-2, CO_2, and CH_4 storage. Polymer Chemistry 2011; 2: 2775-2777.

31. Dawson R, Adams DJ, Cooper AI. Chemical tuning of CO_2 sorption in robust nanoporous organic polymers. Chemical Science 2011; 2: 1173-1177.

32. Li P-Z, Zhao Y. Nitrogen-rich porous adsorbents for CO_2 capture and storage. Chemistry – An Asian Journal 2013; 8: 1680-1691.

33. Erdogan FO. Freundlich, Langmuir, Temkin, DR and Harkins-Jura isotherm studies on the adsorption of CO_2 on various porous adsorbents. International Journal of Chemical Reactor Engineering 2019; 17.

34. Furukawa H, Yaghi OM. Storage of hydrogen, methane, and carbon dioxide in highly porous covalent organic frameworks for clean energy applications. Journal of the American Chemical Society 2009; 131: 8875-8883.

35. Germain J, Svec F, Fréchet JMJ. Preparation of size-selective nanoporous polymer networks of aromatic rings: potential adsorbents for hydrogen storage. Chemistry of Materials 2008; 20: 7069-7076.

36. Jiang J-X, Su F, Trewin A, Wood CD, Niu H et al. Synthetic control of the pore dimension and surface area in conjugated microporous polymer and copolymer networks. Journal of the American Chemical Society 2008; 130: 7710-7720.

37. Oguz Erdogan F, Kopac T. Comparison of activated carbons produced from zonguldak kozlu and zonguldak karadon hard coals for hydrogen sorption. Energy Sources, Part A: Recovery Utilization and Environmental Effects 2020; 1-17.

38. Tozawa T, Jones JTA, Swamy SI, Jiang S, Adams DJ et al. Porous organic cages. Nature Materials 2009; 8: 973.

39. Rabbani MG, Sekizkardes AK, El-Kadri OM, Kaafarani BR, El-Kaderi HM. Pyrene-directed growth of nanoporous benzimidazole-linked nanofibers and their application to selective CO_2 capture and separation. Journal of Materials Chemistry 2012; 22: 25409-25417.

40. Mastalerz M, Hauswald H-JS, Stoll R. Metal-assisted salphen organic frameworks (MaSOFs) with high surface areas and narrow pore-size distribution. Chemical Communications 2012; 48: 130-132.

41. Katsoulidis AP, Kanatzidis MG. Mesoporous hydrophobic polymeric organic frameworks with bound surfactants. selective adsorption of C_2H_6 versus CH_4. Chemistry of Materials 2012; 24: 471-479.

42. Rabbani MG, El-Kaderi HM. Synthesis and characterization of porous benzimidazole-linked polymers and their performance in small gas storage and selective uptake. Chemistry of Materials 2012; 24: 1511-1517.

43. Oguz Erdogan F. A comparative study on methane adsorption onto various adsorbents including activated carbons, zeolites, MWCNT, and MCM-41. International Journal of Coal Preparation and Utilization 2020; 1-21.

44. Oguz Erdogan F. Carbon dioxide and methane adsorption behaviour of zeolite/biomass-based activated carbon and zeolite/multiwalled carbon nanotube composites. International Journal of Environmental Analytical Chemistry 2020; 1-19.

45. Myers AL, Prausnitz JM. Thermodynamics of mixed-gas adsorption. AIChE Journal 1965; 11: 121-127.

46. Yang X, Yu M, Zhao Y, Zhang C, Wang X et al. Hypercrosslinked microporous polymers based on carbazole for gas storage and separation. RSC Advances 2014; 4: 61051-61055.

47. Xie Y-F, Ding S-Y, Liu J-M, Wang W, Zheng QY. Triazatruxene based covalent organic framework and its quick-response fluorescence-on nature towards electron rich arenes. Journal of Materials Chemistry C 2015; 3: 10066-10069.

48. Zhu Y, Long H, Zhang W. Imine-linked porous polymer frameworks with high small gas (H2, CO2, CH4, C2H2) uptake and CO2/N2 selectivity. Chemistry of Materials 2013; 25: 1630-1635.

49. Yang X, Yao S, Yu M, Jiang J-X. Synthesis and gas adsorption properties of tetra-armed microporous organic polymer networks based on triphenylamine. Macromolecular Rapid Communications 2014; 35: 834-839.

50.   Wang ZG, Liu X, Wang D, Jin J. Tröger's base-based copolymers with intrinsic microporosity for CO2 separation and effect of Tröger's base on separation performance. Polymer Chemistry 2014; 5: 2793-2800.

51.   Qiao S, Du Z, Yang R. Design and synthesis of novel carbazole–spacer–carbazole type conjugated microporous networks for gas storage and separation. Journal of Materials Chemistry A 2014; 2: 1877-1885.

52.   Zhang X, Lu J, Zhang J. Porosity enhancement of carbazolic porous organic frameworks using dendritic building blocks for gas storage and separation. Chemistry of Materials 2014; 26: 4023-4029.

53.   Nguyen TS, Yavuz CT. Quantifying the nitrogen effect on CO2 capture using isoporous network polymers. Chemical Communications 2020; 56: 4273-4275.

Supporting Information

Content   Page

1. General methods and characterization

All reagents were purchased from commercial supplier (Sigma-Aldrich Corp.) and used without further purification. Solid-state NMR measurements were carried out with Bruker Ascend 400 MHz spectrometer (Billerica, Massachusetts, ABD). The ^{13}C CP/MAS NMR spectra were obtained with a 4-mm double-resonance MAS probe and with a sample spinning rate of 8.0 kHz; a contact time of 2 ms and pulse delay of 3 s were acquired. The gas adsorption and desorption experiments were performed using Micromeritics 3Flex system. The samples were degassed at 200 °C for 12 h before the measurements. Surface areas were determined from the adsorption data using Brunauer–Emmett–Teller (BET) and Langmuir methods. The pore-size-distribution curves were obtained from the adsorption curve using nonlocal density functional theory (NLDFT) method. Scanning & Transmission Electron Microscopy (SEM & STEM) images were obtained Hitachi SU-5000 (Chiyoda, Tokyo, Japan) microscope worked at changing voltage of 5.0 – 30.0 kV. The thermal behaviour of polymer materials was investigated thermogravimetric analysis (TGA) instrument (Eixstar) over the temperature range of 20 to 800 °C under N_2 atmosphere. FTIR spectra were recorded with Bruker Alpha-P instrument. Powder X-ray diffraction (PXRD) results were obtained with Shimadzu XRD 6000 (Shimadzu Scientific Instruments Incorporated, Kyoto, Japan) operated at 40 kV and 40 mA with Cu Kα radiation (step size: 0.020, step time: 0.60 s).

2. Synthetic procedures

2.1. 10,15-Dihydro-5H-diindolo[3,2-a:3',2'-c]carbazole (Triazatruxene, 2)

In a 50 mL round-bottomed flask there was added 2-oxoindole (1; 2 g, 15 mmol) into $POCl_3$ (10 mL, 105 mmol) stirred until dissolved at RT then stirred at 100 °C for 8 h. After 8 h, reaction mixture was cooled to room temperature and poured into a 500 mL beaker containing ice chips (250 mL) and saturated KOH was added until pH value is 7. The resulting dark green colored settlings was collected by vacuum filtration using No. 2 sintered glass filtrate and the raw product (1.2 g) was purified by silica gel (150 g) column chromatography by using 4:1 Ethyl acetate/hexane as the eluent. After crystallization from 4:1 acetone/hexane, 10,15-dihydro-5*H*-diindolo[3,2-*a*:3',2'-*c*]carbazole (2) was obtained (Yield: 40%, 0.8 g)[23]. Melting point: 393–394 °C. ^{1}H-NMR (600 MHz, DMSO): δ 11.86 (bs, 3H), 8.67 (d, *J* = 7.6 Hz, 3H), 7.73 (d, *J* = 7.6 Hz, 3H), 7.40–7.32 (m, 6H). APT ^{13}C-NMR (150 MHz, DMSO): δ 139.0, 134.2, 123.0, 122.7, 120.3, 119.5, 111.4, 101.0. IR (KBr, cm^{-1}): 3473, 3439, 3053, 3025, 2919, 2852, 1737, 1635, 1273, 729.

2.2. 5,10,15-triethyl-10,15-dihydro-5H-diindolo[3,2-a:3',2'-c]carbazole (3)

In a 100 mL anhydrous THF, triazatruxene (2; 1.85 g, 5.36 mmol) and KOH (4.51 g, 80.34 mmol, 15 eq.) was added at room temperature and mixture was heated at 70 °C for 3.5 h. After cooling the room temperature, ethyl bromide (2.33 g, 21.42 mmol, 4eq.) was added to the mixture. The mixture was stirred magnetically overnight at room temperature. After checking with TLC and understanding that the reaction was complete, solvent was removed under reduced pressure. The raw product was dissolved in 150 mL of EtOAc and washed with diluted $NaHCO_3$ (1×100 mL) then water (3×100 mL) and dried over $MgSO_4$. The solvent was removed under reduced pressure. The raw product was purified on silica gel (20 g) column chromatography by using 1:4 CH_2Cl_2/hexane. After crystallization over acetone, 5,10,15-triethyl-10,15-dihydro-5H-diindolo[3,2-a:3',2'-c]carbazole (3) was obtained. (Yield: 89%, 2.1 g) ^{1}H-NMR (600 MHz, CDCl$_3$): δ ppm 8.37 (d, J = 8.0 Hz, 3H), 7.68 (d, J = 8.0 Hz, 3H), 7.48 (t, J = 7.4 Hz, 3H), 7.37 (t, J = 7.4 Hz, 3H), 5.05 (t, J = 7.2 Hz, 6H), 1.64 (t, J = 7.2 Hz, 9H). ^{13}C-NMR (150 MHz, CDCl$_3$): δ ppm 143.4, 141.4, 126.2, 125.4, 124.1, 122.5, 113.0 105.9, 44.4, 18.2. IR (powder, cm^{-1}): 3045, 2970, 1555, 1480, 1320, 1233, 1098, 724. HRMS: m/z: Calcd. for ($C_{30}H_{27}N_3$) [M+H$^+$]: 430.22385; found, 430.22868.

2.3. Synthesis of TATHCCP

In 20 mL nitrobenzene, 5,10,15-triethyl-10,15-dihydro-5H-diindolo[3,2-a:3',2'-c]carbazole (3) (0.250 g, 0.582 mmol) and *p*-dimethoxybenzene (1.210 g, 8.73 mmol, 15 equiv.) in 20 mL 1,2-dichloroethane, anhydrous $FeCl_3$ (4.150 g, 25.61 mmol, 44 equiv.) was added at room temperature. The mixture was stirred at 80 °C for 5 h then 120°C for 24 h under an inert (N_2) atmosphere. After 24 h, reaction mixture was cooling to room temperature then the dark brown precipitate was collected by using No. 1 sintered glass filtrate and repeatedly washed with methanol, concentrated HCl, and distilled water to eliminate unreacted monomers and $FeCl_3$ till the filtrate was almost colorless. After that the TATHCCP was purified by Soxhlet extraction from THF (50 mL) for 24 h then dried under vacuum at 120 °C for 24 h to give dark brown-colored solid powder (Yield: 551 mg, 97 %). IR (powder, cm^{-1}): 2927, 1572, 1457, 1427, 1324, 1208, 1135, 852, 811.
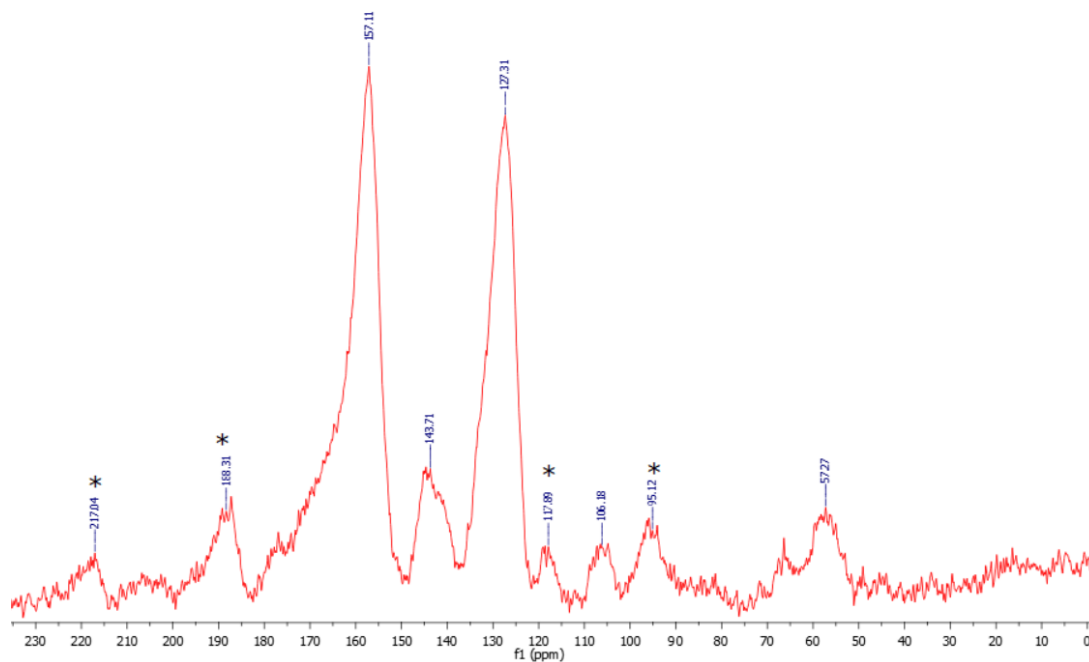
3. General spectra of TATHCCP

Figure S1. (CP/MAS) ^{13}C NMR spectra of TATHCCP**.**
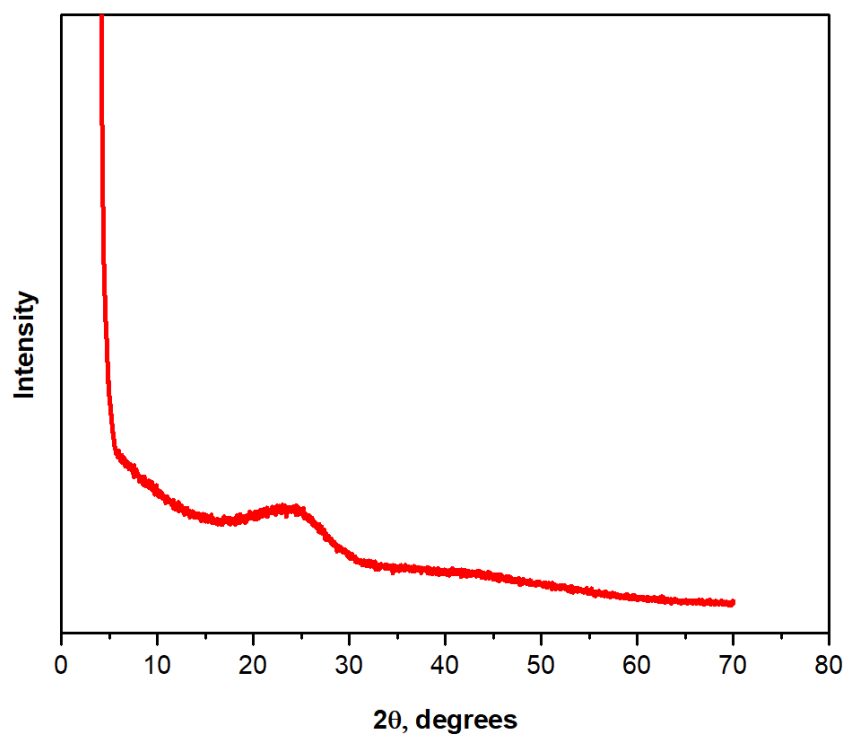

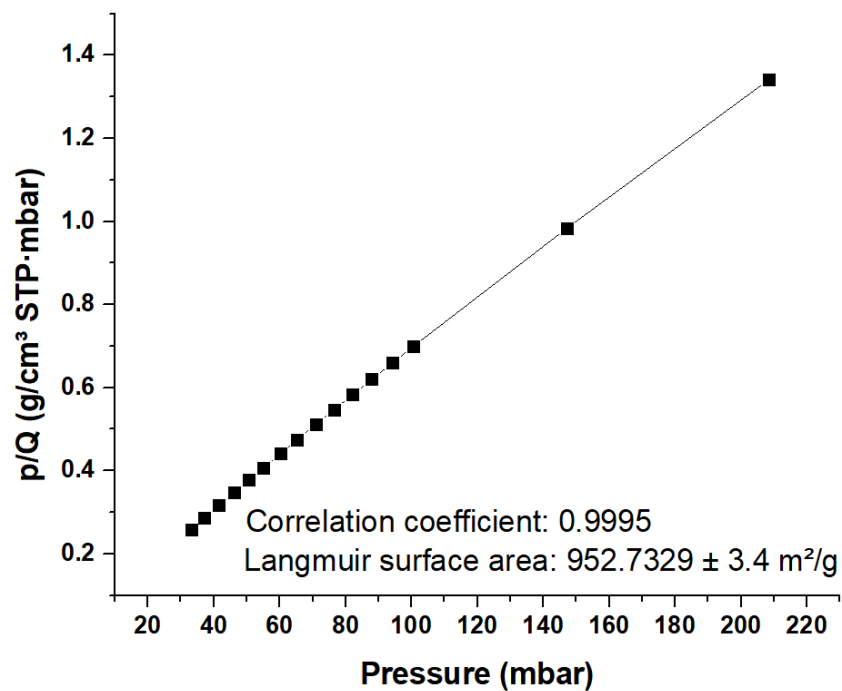**Figure S2.** PXRD pattern profile of TATHCCP**.**

4

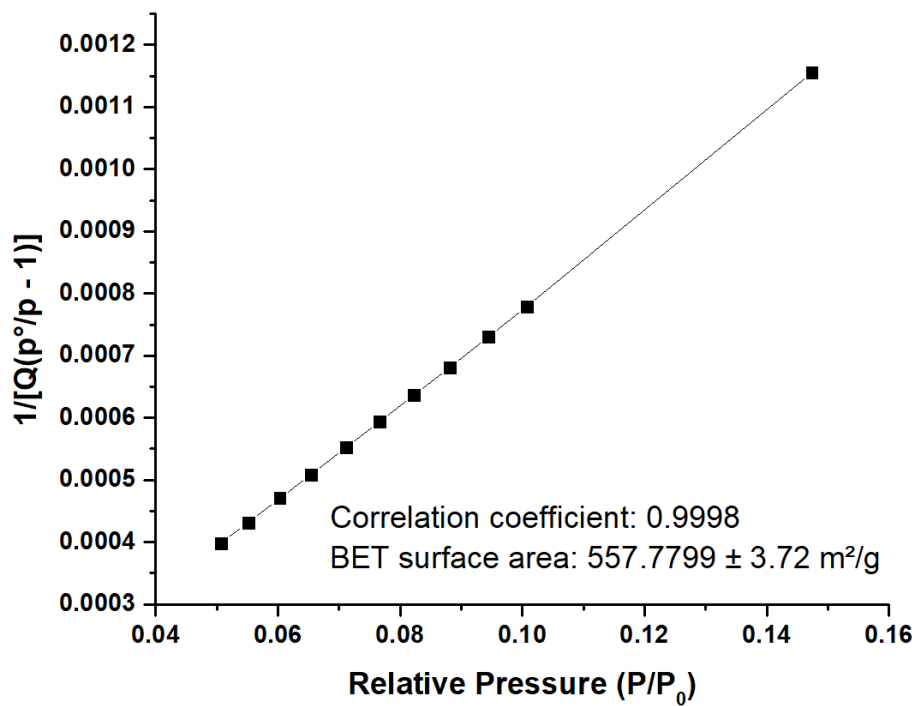**Figure S3.** Langmuir surface area plot for TATHCCP calculated from the isotherm.

Figure S4. BET surface area plot for TATHCCP calculated from the isotherm.

Table S1. Comparable gas adsorption capacity of the TATHCCP with TATHCP.

Gas/Temperature	273 (K)	298(K)	323(K)
CO_2 wt %	9 / 12.55	5.5 / 7.68	3.2 / 4.75
CH_4 wt %	1.06 / 1.56	0.62 / 0.90	0.37 / 0.60
O_2 wt %	0.61 / 0.88	0.36 / 0.48	0.22 / 0.31
CO wt %	0.75 / 1.04	0.43 / 0.58	0.26 / 0.38
N_2 wt %	0.52 / 0.92	0.30 / 0.03	0.18 / 0.02
H_2 wt % (77K)	0.84 / 1.30	-	-

Table S2. Comparable results of gas selectivity for TATHCCP with TATHCP.

Gases/ Temperature	273K	298K	323K
CO_2/N_2 (05/95)	49.2	25.9	18.2
CO_2/N_2 (15/85)	50.0 / 38.4	25.9 / 22.3	18.3 / 15.3
CO_2/N_2 (50/50)	59.1 / 37.5	28.5 / 24.1	18.3 / 15.6
CO_2/CH_4 (50/50)	12.3 / 7.8	5.4 / 5.2	4.4 / 4.2
CO_2/CH_4 (5/95)	9.7 / 7.9	5.9 / 4.8	4.5 / 4.1
CO_2/O_2 (50/50)	45.9 / 40.6	23.5 / 25.5	16.4 / 18.0
CO_2/CO (50/50)	35.0 / 32.1	17.6 / 18.6	12.3 / 13.2

Table S3. Comparison of different microporous materials with respect to their textural and CO_2 uptake (wt % - mmol) values.

Material	BET (m^2/g^{-1})	CO_2 uptake (wt %-mmol) at 273K	CO_2 uptake (wt %/mmol) at 298K
TATHCCP	557	9 / 2.1	5.5 / 1.27
TATHCP[1]	957	12.6	7.7
YBN-CC[2]	579	8.78 / 2.0	5.61 / 1.27
YBN-DMM[2]	784	12.70 / 2.87	7.70 / 1.75
YBN-DMB[2]	968	12.74 / 2.87	7.41 / 1.68
PAF-1[3]	5600	9.1	-
PON-1[4]	1400	10.8	-
TPI-1[5]	809	10.7	-
BPL carbon	-	9.15	-
IN[4]	243	7.5	4.85
BT[4]	571	10.6	6.4
BF[4]	1022	10.6	6.0
PECONF-2[6]	637	12.5	8.7
PECONF-4[6]	-	0.6	7.9
BLP-1H at [7]	-	7.4	-
COF-103[8]	-	7.6	-
CMP-1[8]	-	9.02	-
CBZ[4]	391	9.2	6.02
DBT[4]	493	9.7	6.06
BILP-1[13]	1172	4.27mmol	2.97mmol
BILP-2[13]	708	3.39mmol	2,36mmol
BILP-3[13]	1306	5.11mmol	3.29mmol
BILP-5[13]	599	2.9mmol	1.97mmol
ALP-1[25]	1235	5,36mmol	3.24mmol
ALP-4[25]	862	3.5mmol	1.84mmol

Table S4. Comparison of different microporous materials with respect to their H_2 uptake. (wt %) values.

Material	H_2 uptake (wt%) at 77K
TATHCCP	0.84
TATHCP[1]	1.30
YBN-CC[2]	1.59
YBN-DMM[2]	1.23
YBN-DMB[2]	1.18
Polyaniline[16]	0.85
CMP-2[17]	0.91
COF-103[8]	1.25

Table S5. Comparison of different microporous materials with respect to their CH_4 uptake (wt %) values.

Material	CH_4 uptake (wt%) at 273K
TATHCCP	1.06
TATHCP[1]	1.56
YBN-CC[2]	1.08
YBN-DMM[2]	1.61
YBN-DMB[2]	1.47
DBF[4]	1.47
BT[4]	1.34
BF[4]	1.22
CBZ[4]	1.16
IN[4]	0.73
MaSOF-1[10]	0.98
SBICC[11]	0.98
mesoPOF-1[12]	1.49
BILP-5[13]	1.77
BILP-10[14]	1.61
CC2[15]	1.82

Table S6. Comparison of different microporous materials with respect to their CO_2/N_2 (15/85) selectivity values at 273 K.

Material	Selectivity
TATHCCP	50
TATHCP[1]	38.4
YBN-CC[2]	60.0
YBN-DMM[2]	44.6
YBN-DMB[2]	159.1
FCBZz[18]	28.9
FCTCz[18]	26.1
TATCOF2[19]	5.9
YPTPA[20]	17.3
SPTPA[20]	30.6
TBPIM33[21]	18.1
TBPIM25[21]	17.0
PPF-1[22]	14.5
PPF-2[22]	15.4
PPF-3[22]	20.4
PPF-4[22]	15.0

Table S7. Comparison of different microporous materials with respect to their CO_2/CH_4 (50/50) selectivity values at 273 K.

Material	Selectivity
TATHCCP	9.7
TATHCP[1]	7.8
YBN-CC[2]	7.9
YBN-DMM[2]	6.9
YBN-DMB[2]	7.3
FCBZ[18]	5.8
FCTCz[18]	5.2
CMPs[23]	4
Cz-POF1[24]	4.4
Cz-POF3[24]	4.7
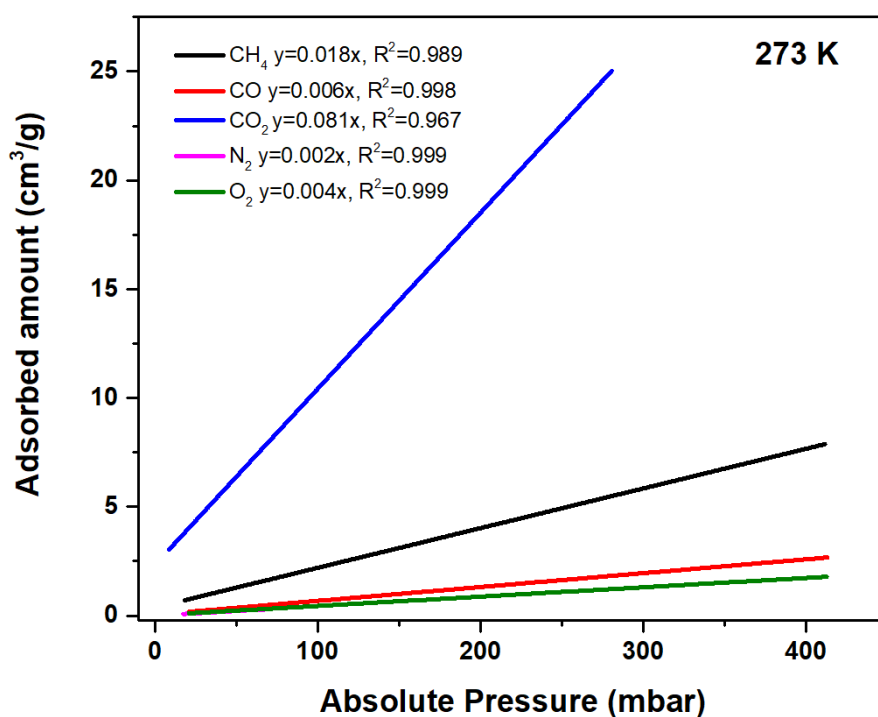
Figure S5. Initial slope fitting for gases of TATHCCP at 273K
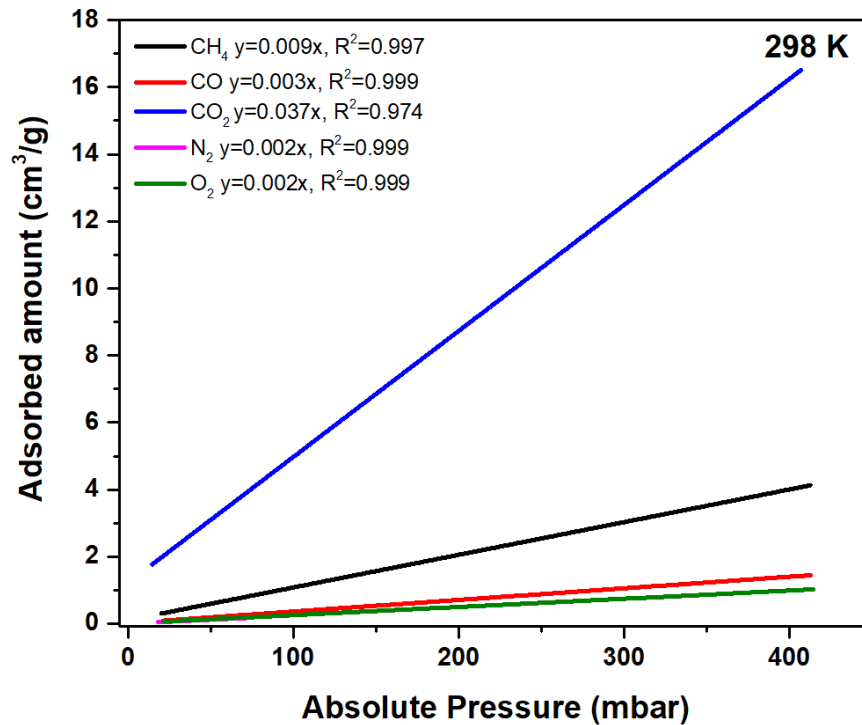
Figure S6. Initial slope fitting for gases of TATHCCP at 298K.
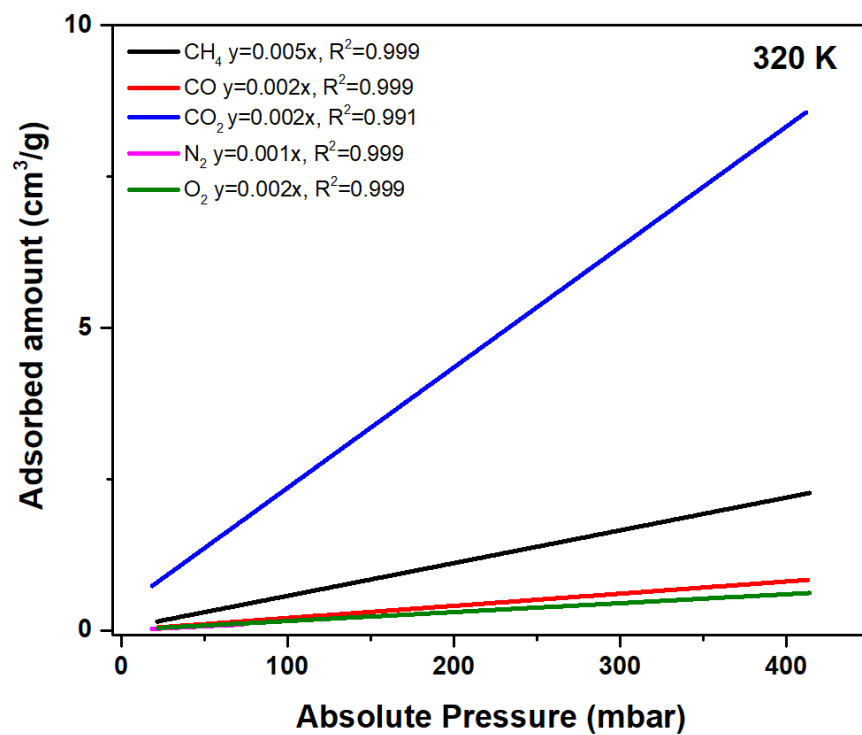
Figure S7. Initial slope fitting for gases of TATHCCP at 320 K.
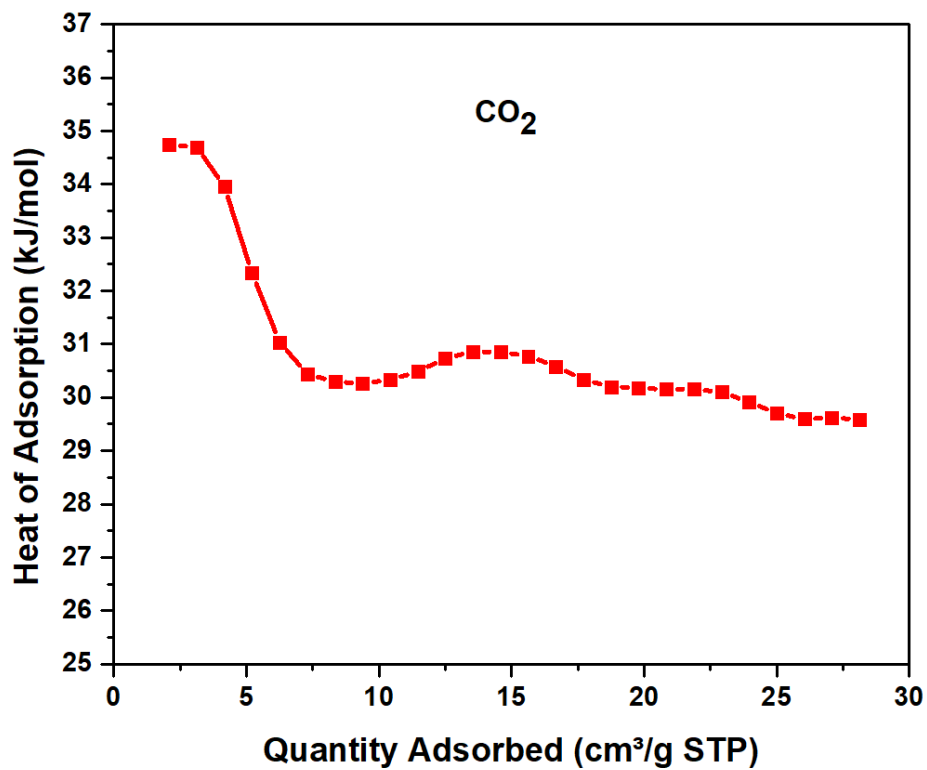
Figure S8. The isosteric heat of adsorption (Q_{st}) of TATHCCP for CO_2.
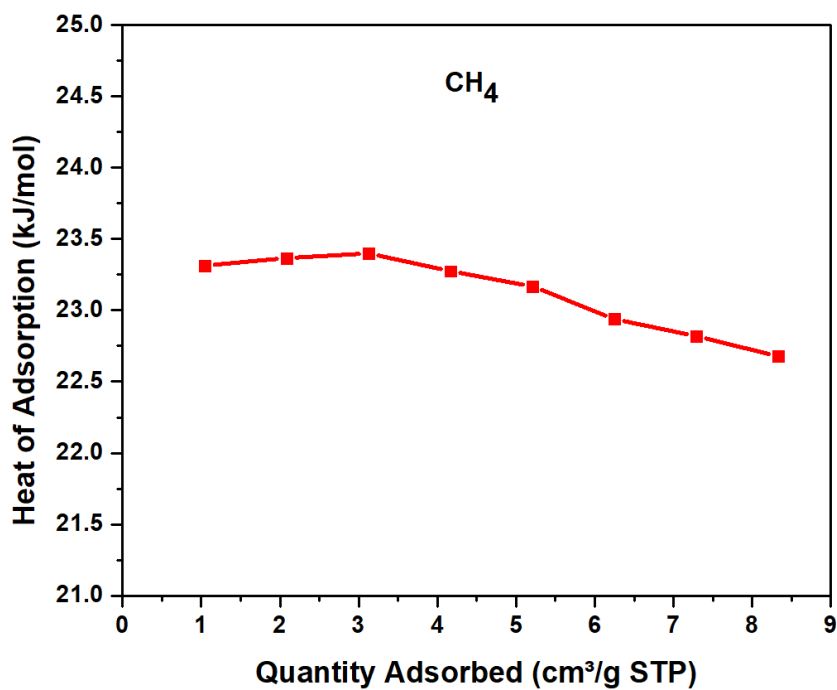
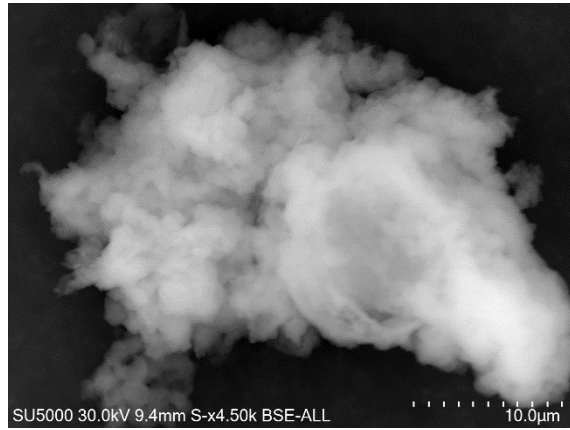**Figure S9.** The isosteric heat of adsorption (Q_{st}) of TATHCCP for CH_4.
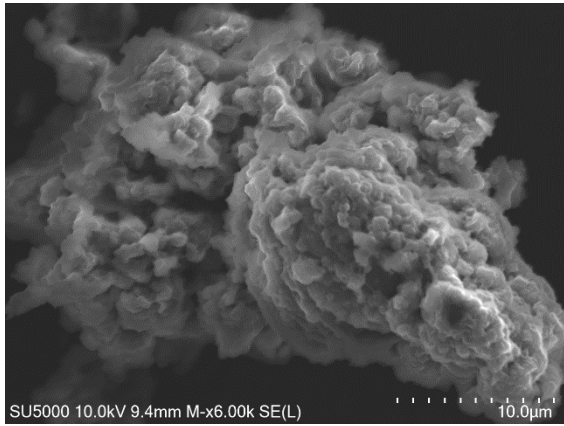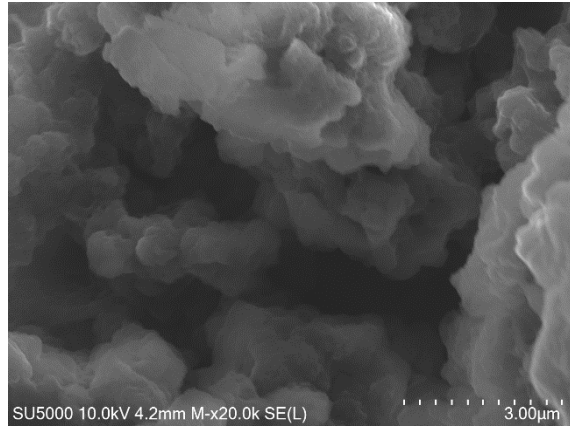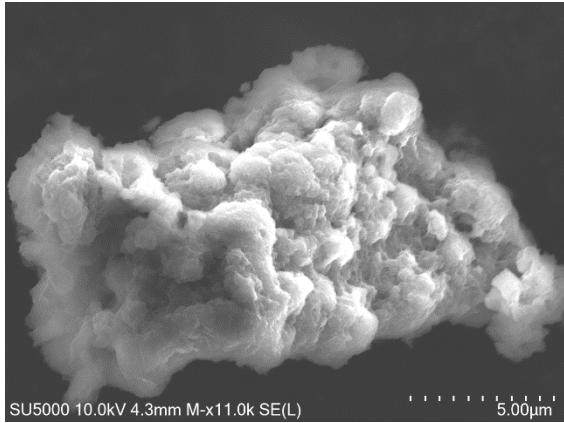
10
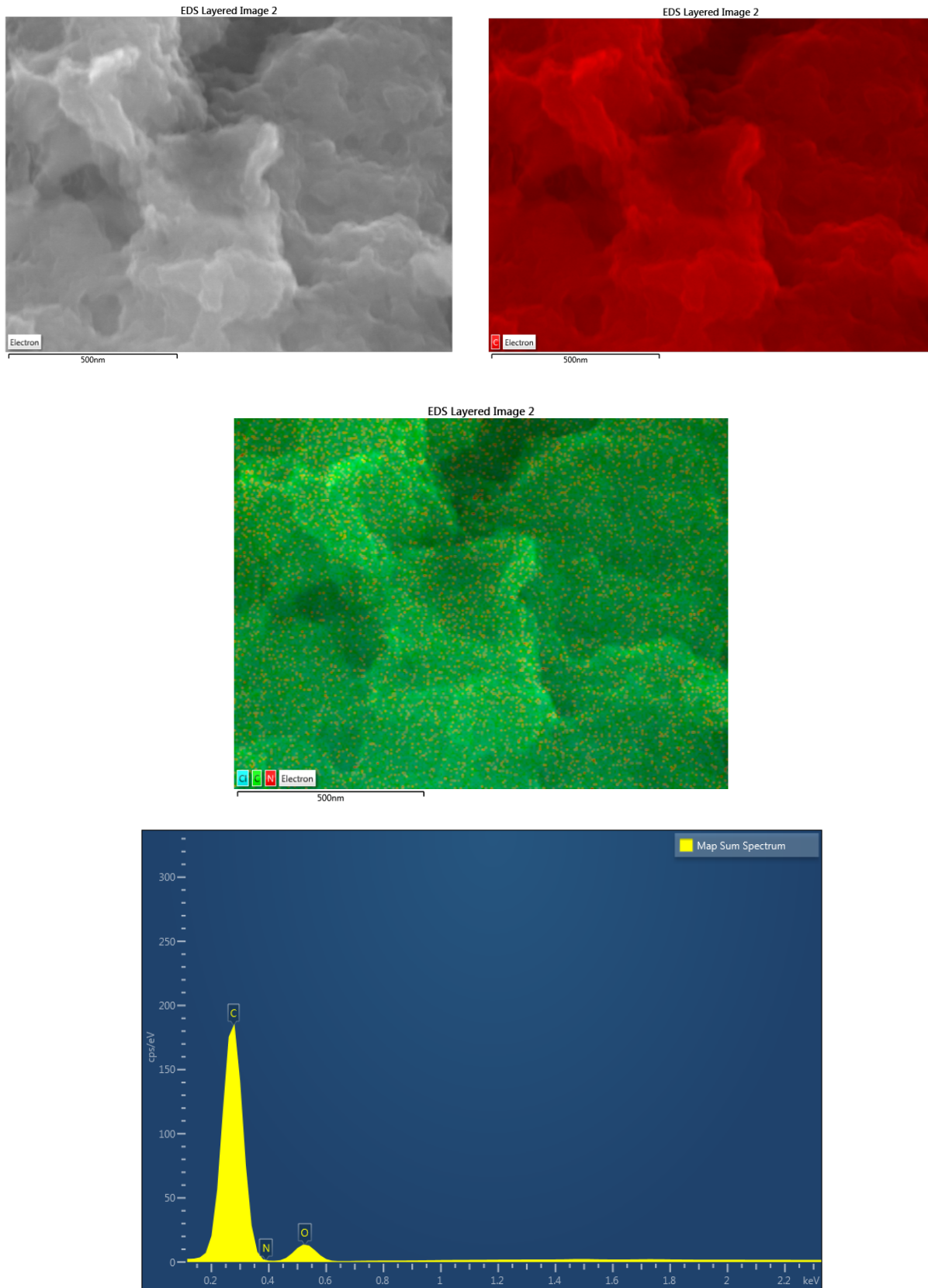
Figure S10. EDS spectra of TATHCCP.

4. Scanning electron microscopy (SEM) images of TATHCCP
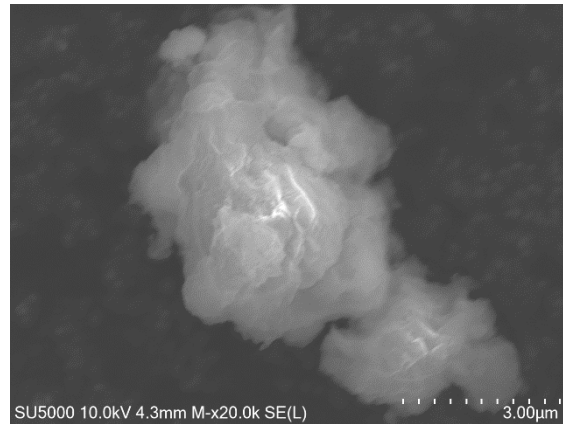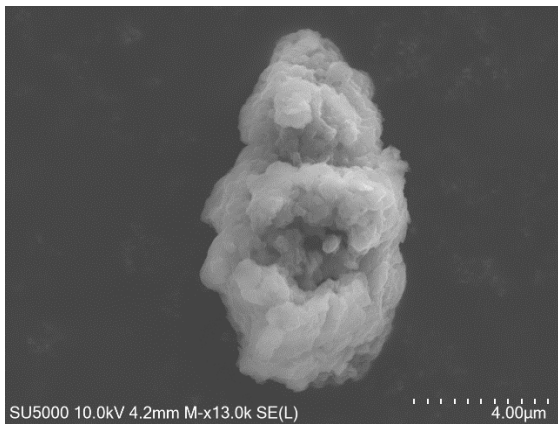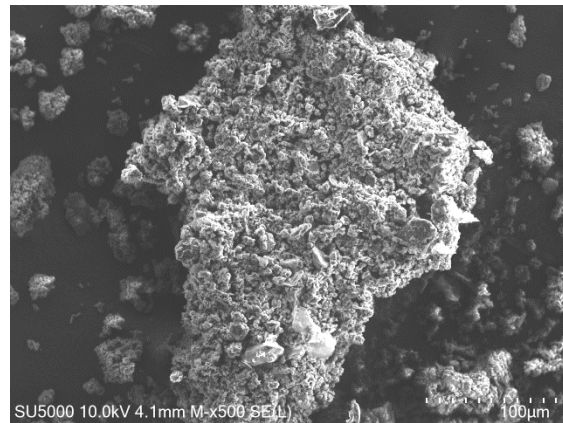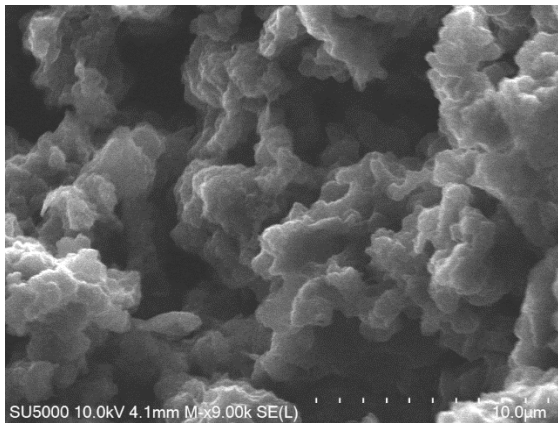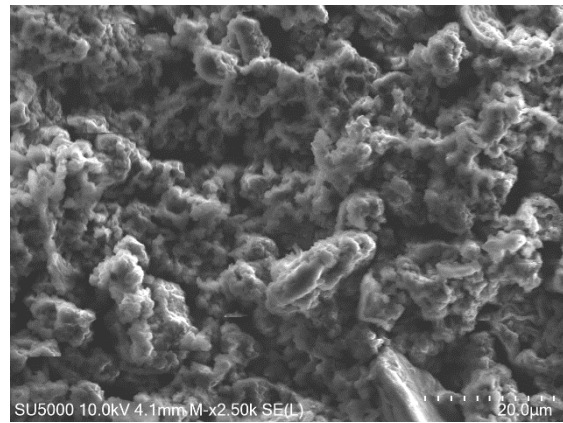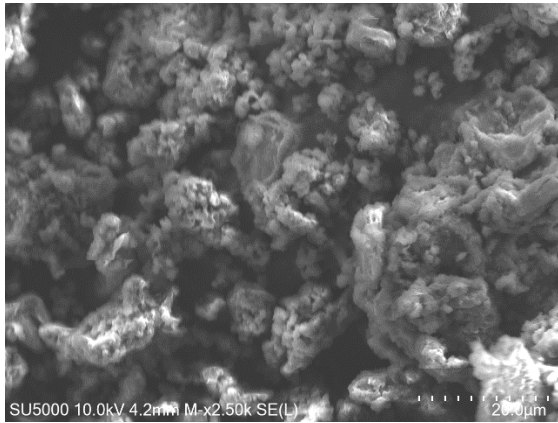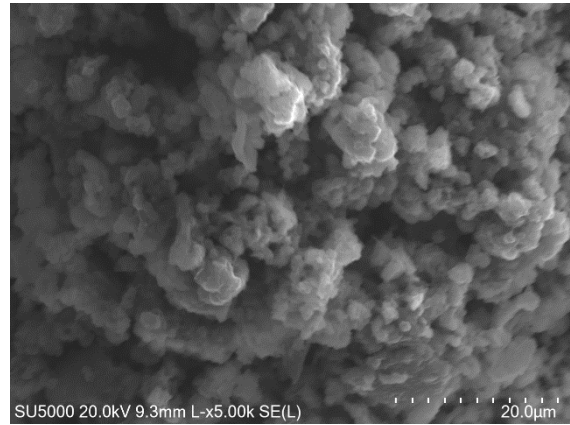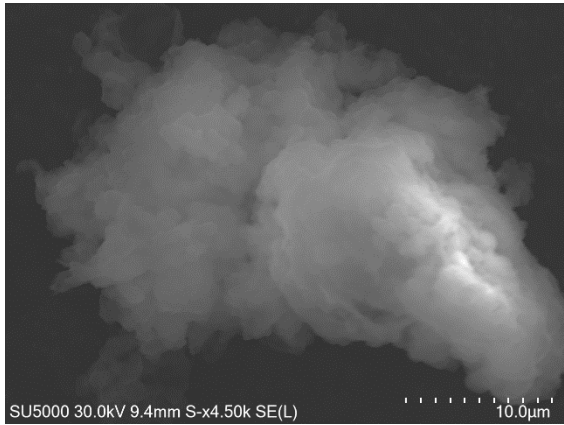
5. References

1. Sadak AE, Karakuş E, Chumakov YM, Dogan NA, Yavuz CT. Triazatruxene-based ordered porous polymer: high capacity CO2, CH4, and H2 capture, heterogeneous Suzuki–Miyaura catalytic coupling, and thermoelectric properties. ACS Applied Energy Materials 2020; 3: 4983-4994.
2. Sadak AE. A comparative gas sorption study of dicarbazole-derived microporous hyper-crosslinked polymers. Microporous and Mesoporous Materials 2021; 311: 110727.
3. T. Ben, C. Pei, D. Zhang, J. Xu, F. Deng X et al. Gas storage in porous aromatic frameworks (PAFs). Energy Environmental Science 2011, *4*, 3991-3999.
4. Jeon HJ, Choi JH, Lee Y, Choi KM. Park JH, Kang JK. Highly selective CO2-capturing polymeric organic network structures. Advanced Energy Materials 2012, *2*, 225-228.
5. Liebl M. R., Senker J. Microporous Functionalized Triazine-Based Polyimides with High CO2 Capture Capacity. Chemistry of Materials 2013, *25*, 970-980.
6. Mohanty P, Kull LD, Landskron K. Porous covalent electron-rich organonitridic frameworks as highly selective sorbents for methane and carbon dioxide. Nature Communications 2011,*2*, 401-406.
7. Jackson KT, Rabbani MG, Reich TE, El-Kaderi HM; Synthesis of highly porous borazine-linked polymers and their application to H2, CO2, and CH4 storage. Polymer Chemistry 2011, *2*, 2775-2777.
8. Furukawa H, and Yaghi OM. Storage of hydrogen, methane, and carbon dioxide in highly porous covalent organic frameworks for clean energy applications. Journal of the American Chemical Society 2009, 131, 8875–8883.
9. Dawson R, Adams DJ, Cooper AI. Chemical tuning of CO2sorption in robust nanoporous organic polymers. Chemical Science 2011, 2, 1173–1177.
10. Mastalerz M, Hauswald HJS, Stoll R. A shape-persistent exo-functionalized [4 + 6] iminecage compound with a very high specific surface area. Chemical Communications 2012, 48, 130-132.
11. Germain J, Svec F, Fréchet JMJ. Preparation of Size-Selective Nanoporous Polymer Networks of Aromatic Rings: Potential Adsorbents for Hydrogen Storage. Chemistry of Materials 2008, *20*, 7069-7076.
12. Katsoulidis AP, Kanatzidis MG. Mesoporous hydrophobic polymeric organic frameworks with bound surfactants. selective adsorption of C2H6 versus CH4. Chemistry of Materials 2012, 24, 471-479.
13. Rabbani MG, El-Kaderi HM. Synthesis and characterization of porous benzimidazole-linked polymers and their performance in small gas storage and selective uptake. Chemistry of Materials 2012; 24: 1511-1517.
14. Rabbani MG, Sekizkardes AK, El-Kadri OM, Kaafarani BR, El-Kaderi HM. Pyrene-directed growth of nanoporous benzimidazole-linked nanofibers and their application to selective CO2 capture and separation. Journal of Materials Chemistry 2012, 22: 25409-25417.
15. Tozawa T, Jones JT, Swamy SI, Jiang S, Adams DJ et al. Porous organic cages. Nature materials 2009; 8(12), 973-978.
16. Germain J, Svec F, Fréchet JM. Preparation of size-selective nanoporous polymer networks of aromatic rings: potential adsorbents for hydrogen storage. Chemistry of Materials 2008, 20(22), 7069-7076.
17. Jiang JX, Su F, Trewin A, Wood CD, Niu H et al. Synthetic control of the pore dimension and surface area in conjugated microporous polymer and copolymer networks. Journal of the American Chemical Society 2008, 130(24), 7710-7720.
18. Yang X, Yu M, Zhao Y, Zhang C, Wang X et al. Hypercrosslinked microporous polymers based on carbazole for gas storage and separation. RSC Advances 2014, 4(105), 61051-61055.
19. Xie YF, Ding SY, Liu JM, Wang W, Zheng QY. Triazatruxene based covalent organic framework and its quick-response fluorescence-on nature towards electron rich arenes. Journal of Materials Chemistry C 2015, 3(39), 10066-10069
20. Yang X, Yao S, Yu M, Jiang JX. Synthesis and gas adsorption properties of tetra-armed microporous organic polymer networks based on triphenylamine. Macromolecular Rapid Communications 2014, 35(8), 834-839.
21. Wang ZG, Liu X, Wang D, Jin J. Tröger's base-based copolymers with intrinsic microporosity for CO 2 separation and effect of Tröger's base on separation performance. Polymer Chemistry 2014, 5(8), 2793-2800.
22. Zhu Y, Long H, Zhang W. Imine-linked porous polymer frameworks with high small gas (H2, CO2, CH4, C2H2) uptake and CO2/N2 selectivity. Chemistry of Materials 2013, 25(9), 1630-1635.
23. Qiao S, Du Z, Yang R. Design and synthesis of novel carbazole–spacer–carbazole type conjugated microporous networks for gas storage and separation. Journal of Materials Chemistry A 2014, 2(6), 1877-1885.

24. Chen Q, Luo M, Hammershøj P, Zhou D, Han Y et al. Microporous polycarbazole with high specific surface area for gas storage and separation. Journal of the American Chemical Society 2012, 134(14), 6084-6087.
25. Arab P, Rabbani MG, Sekizkardes AK, İslamoğlu T, El-Kaderi HM. Copper (I)-catalyzed synthesis of nanoporous azo-linked polymers: impact of textural properties on gas storage and selective carbon dioxide capture. Chemistry of Materials 2014, 26(3), 1385-1392.